



Research articles

Magnetic properties of ordered arrays of iron nanowires: The impact of the length

A.H.A. Elmekawy^{a,b}, E. Iashina^c, I. Dubitskiy^c, S. Sotnichuk^{a,d}, I. Bozhev^{e,f}, D. Kozlov^{d,g}, K. Napolskii^{d,h}, D. Menzelⁱ, A. Mistonov^{a,*}^a St. Petersburg State University, Department of Physics, 198504 St. Petersburg, Russia^b Cyclotron Project, Nuclear Research Center, Atomic Energy Authority, 13759 Cairo, Egypt^c Petersburg Nuclear Physics Institute named by B. P. Konstantinov of National Research Centre Kurchatov Institute, 188300 Gatchina, Leningrad Region, Russia^d M. V. Lomonosov Moscow State University, Department of Materials Science, 119991 Moscow, Russia^e M. V. Lomonosov Moscow State University, Department of Physics, 119991 Moscow, Russia^f M. V. Lomonosov Moscow State University, Quantum Technology Centre, 119991 Moscow, Russia^g Kurnakov Institute of General and Inorganic Chemistry of the Russian Academy of Sciences, 119991 Moscow, Russia^h M. V. Lomonosov Moscow State University, Department of Chemistry, 119991 Moscow, Russiaⁱ Institute of Condensed Matter Physics, 308108 Braunschweig, Germany

ARTICLE INFO

Keywords:

Ferromagnetic nanowire arrays

Iron nanowires

Anodic alumina

First-order reversal curve

SQUID-magnetometry

2020 MSC:

00-01

99-00

ABSTRACT

The present study is focused on the investigation of the magnetic properties of hexagonally ordered iron nanowire arrays electrodeposited into anodic alumina templates. A series of 9 arrays of nanowires with a diameter of 52 nm, an interwire distance of 100 nm, and a length varying from 3.6 to 21.2 μm is analyzed. Scanning electron microscopy, X-ray diffraction, SQUID magnetometry, and first-order reversal curves (FORC) analysis are used for the characterization of the nanowire arrays. The increase in coercivity with nanowire length is well described by a model of interacting wires, which are magnetized likely by a vortex domain wall mechanism. According to the width of distribution observed in the FORC diagrams, interaction fields decrease with increasing length, which supports the proposed model.

1. Introduction

Magnetic nanowire arrays (MNA) are of great interest owing to their possible applications and fundamental challenges [1–3]. Modern inexpensive synthesis techniques allow for production of high-quality structures with well-controlled preparation parameters [4]. However, the absence of a complete understanding of the correlation between these parameters and the magnetic properties of the arrays requires plenty of new studies.

The magnetic behavior of MNA is determined by the properties of an individual wire as well as the interaction between the nanowires. The former includes wire shape anisotropy, which depends on diameter and length, magnetocrystalline anisotropy, specified mostly by the material of the wire, and magnetoelastic anisotropy. Overall, magnetic properties are the result of the interplay between all these terms. Thus, understanding of this interplay opens up a pathway to novel devices based on MNA.

Coercivity and squareness (the ratio of remanent magnetization M_r to saturation magnetization M_s) are widely used to characterize the magnetic behavior. Since shape anisotropy and magnetostatic interactions strongly depend on geometrical parameters of MNA [5], the influence of wire diameter, length, and interwire distance on the coercivity and squareness has been widely addressed [6–11]. On the other hand, the role of magnetocrystalline anisotropy is also crucial and could drastically affect the magnetic properties [12,13]. This leads to a wide diversity of works, devoted to the changes of coercivity upon variation of the composition in multicomponent alloys [14–16].

Using pure Fe as a material for nanowires offers plenty of advantages. It saves one from troubles during alloy deposition. Besides that, Fe possesses a large magnetization, which is important for storage applications, and a cubic crystalline structure exhibiting relatively small magnetocrystalline anisotropy ($K_1 = 48 \text{ kJ/m}^3$). Thus, only shape anisotropy and magnetostatic interactions mostly determine the magnetic behavior of such arrays. A strong disadvantage of Fe is its tendency

* Corresponding author.

E-mail address: a.mistonov@spbu.ru (A. Mistonov).

to oxidize, which has probably made it less studied than Ni [17–21], Co [22–24], and alloys [25–27] in recent years. At the moment, however, synthesis techniques have already overcome this problem [28].

Here we study the dependence of the magnetic properties of Fe-based MNA on the length of nanowires. A model of interacting long wires is exploited to describe the coercivity behavior. Additionally, first-order reversal curves (FORCs) analysis is used in order to scrutinize magnetic interactions in the MNA.

2. Experimental

2.1. Samples preparation

Arrays of Fe nanowires were obtained by templated electrodeposition into porous anodic aluminium oxide (AAO). AAO porous films were prepared by a two-step anodization technique in 0.3 M oxalic acid at constant voltage of 40 V and electrolyte temperature of 0 °C as described elsewhere [29]. The thicknesses of the AAO layers formed at the first and at the second anodization steps were 10 and 35 µm, respectively. In order to remove the barrier oxide layer, the AAO film was etched in 3 M H₃PO₄ with electrochemical detection of the moment when the pores begin to open [30]. To achieve a pore diameter of about 50 nm, the etching process was stopped 30 min after pore opening. Finally, 200-nm-thick Au layer was deposited at the bottom side of the template by magnetron sputtering. Electrodeposition of Fe was performed at room temperature in a three-electrode cell from an electrolyte containing 0.5 M FeSO₄, 0.5 M Na₂SO₄, 0.4 M H₃BO₃ and 0.006 M C₆H₈O₆. A Pt ring served as a counter electrode, a saturated (KCl) Ag/AgCl electrode connected with the cell via a Luggin–Habber capillary was used as a reference electrode. During electrodeposition, the electrolyte was intensively agitated in order to remove hydrogen bubbles from the external surface of AAO template. To minimize the possibility of oxidation, a freshly prepared electrolyte was used for the fabrication of each sample. The Fe deposition was performed in potentiostatic mode at –1.0 V. At the first stage of electrodeposition, a potential pulse of –1.2 V was applied for 0.1 s to induce instantaneous nucleation. The length of the nanowires was controlled coulometrically. Using this process, nanowire arrays with lengths ranging from 4 to 21 µm were fabricated.

2.2. Samples characterization

Phase composition of Fe nanowire arrays was analysed using Rigaku D/MAX 2500 X-ray diffractometer. The measurements were performed in Bragg–Brentano geometry using CuK_α radiation ($\lambda = 1.5418 \text{ \AA}$) in the 2θ range from 30 to 120 degrees.

Geometrical parameters of the nanowire arrays (distance between nanowire centers D_{int} , diameter D_p and length L of nanowire) were determined by scanning electron microscopy (SEM) using a Zeiss Merlin Gemini II instrument. In order to obtain the nanowire lengths with higher accuracy, EDX analysis was involved. Fe content maps were recorded at the Fe K_α line by using Oxford Instruments INCA x-act detector. For each sample, several images at different magnification and for different sample areas were made. After that, all images were processed using the *ImageJ* and *Statistics 2D* [31] software, and the final values of D_p , D_{int} , and L were averaged by all images for each sample.

Remagnetization curves were measured using a Quantum Design MPMS-5S SQUID-magnetometer in the field range H from –20 kOe to 20 kOe, applied both parallel and perpendicular to the long axis of the nanowires. Field steps were set to 100 Oe in the range from –1 to 1 kOe, and to 1 kOe at higher fields. All measurements were performed at 300 K.

First-order reversal curves (FORCs) were measured using LakeShore 7410 vibration magnetometer. The conventional procedure of the measurement was exploited as follows. A sample magnetized in a magnetic field $+H_S$ was placed into a certain field H_r , and the magnetic moment M depending on the current field H_b was measured until $+H_S$

was reached again; then H_r was reduced by ΔH_r , followed by the measurement of the next FORC. This procedure continued until H_r reached $-H_S$. Thus, the magnetization of the sample is a function of actual applied external field H_b as well as of H_r . Following the approach of Mayergoyz [32], we calculated the two-dimensional FORC distribution as follows:

$$\rho_{FORC} = \frac{\partial^2 M_{FORC}(H_b, H_r)}{\partial H_b \partial H_r} \quad (1)$$

The measurements were carried out at room temperature with $H_S = 11 \text{ kOe}$ and $\Delta H_r = 170 \text{ Oe}$ only for four samples. The field was applied parallel to the long axis of the nanowires. FORC diagrams in coordinates $H_c^E = (H_b - H_r)/2$ and $H_u = (H_b + H_r)/2$ [33] were plotted employing the software *FORCinel* [34] using a smoothing factor of 4. In order to distinguish the coercivity obtained from SQUID experiments and FORC measurements, the latter is denoted as H_c^F .

3. Results and discussion

X-ray diffraction patterns of Fe-based MNA are presented in Fig. 1. In order to minimize the intensity of reflections corresponding to Au current collector, this layer was removed from the bottom side of the nanocomposites by ion etching. The main diffraction peaks are attributed to Fe bcc phase. Some samples, however, demonstrate the additional peak at $2\theta = 38^\circ$, which can be attributed to Au particles remained after ion etching. Although peaks for Fe and Au are located close to each other, Figure 1b unambiguously shows that (110) and (211) reflections are attributed exactly to iron phase. Any other iron-containing phases were not detected (the weak peaks near 48° correspond to plasticine, which was used for holding the samples during the analysis). It is clearly seen that the intensity of the peaks expectedly decreases with the nanowire length changing from 21.2 to 3.6 µm. The integral intensity ratio of the (110) and (211) peaks is close to the corresponding ratio of bulk α -Fe (PC-PDF 2 Database Sets (1–85) (6–63)) and, thus, implies that the nanowires are polycrystalline without any texturing. Moreover, the ratio between magnetocrystalline anisotropy of Fe and shape anisotropy of nanowires is small even for the shortest nanowires [35]. These facts allow one to exclude magnetocrystalline term from the consideration.

A typical top-view SEM image of the AAO template is presented in Fig. 2a. Although long-range order is mostly absent, locally the pores are arranged hexagonally. Processing of the SEM image reveals a pore diameter distribution and an interpore distance distribution shown in Figs. 2b and 2c, respectively. The values for D_p and D_{int} are close to the averaged (by all images) results and equal to $51 \pm 4 \text{ nm}$ and $100 \pm 10 \text{ nm}$, respectively.

The length of the wires was determined by processing of cross-sectional SEM images of Fe/AAO nanocomposites (Fig. 3, first column) and corresponding EDX maps of Fe distribution (Fig. 3, second column). Most of the nanowires are uniform in length. However, in three of nine samples a bimodal length distribution was observed. In this case the final value was calculated as weighted average, where weight was taken as the fraction of the wires of corresponding length. Errors were set asymmetrical (see figures below). The lengths of nanowires, calculated using Faraday's law from the electric charge passed during Fe electrodeposition, vary from 4 to 21 µm in the series and are in good agreement with the SEM data.

In Fig. 3 (third column) normalized remagnetization curves obtained by SQUID magnetometry are shown. Hysteresis loops measured with the field applied perpendicular to the long axis of wires are almost independent of the nanowire length and result in $H_S \approx 10 \text{ kOe}$. On the contrary, curves measured in the parallel field direction become more rectangular due to increasing shape anisotropy of the nanowire. Although for the shortest wires ($L = 3.6 \text{ \mu m}$) the curves are almost superimposed, the easy axis of magnetization is parallel to the wire axis.

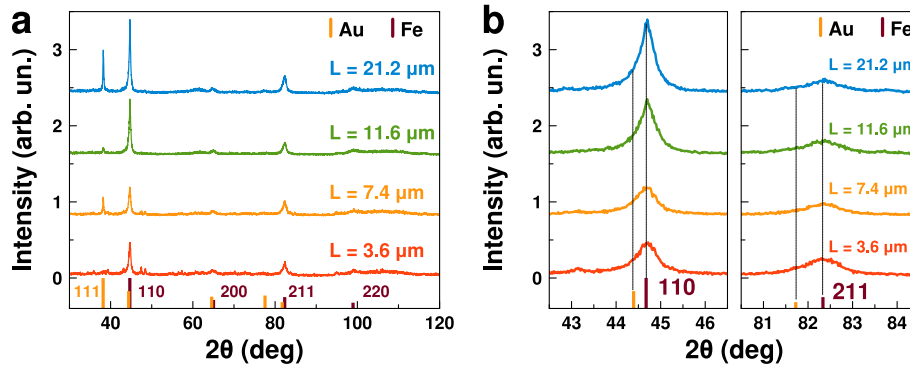


Fig. 1. X-ray diffraction patterns: full range (a), in vicinity of Fe peaks (b). Curves are shifted in vertical direction for clarity.

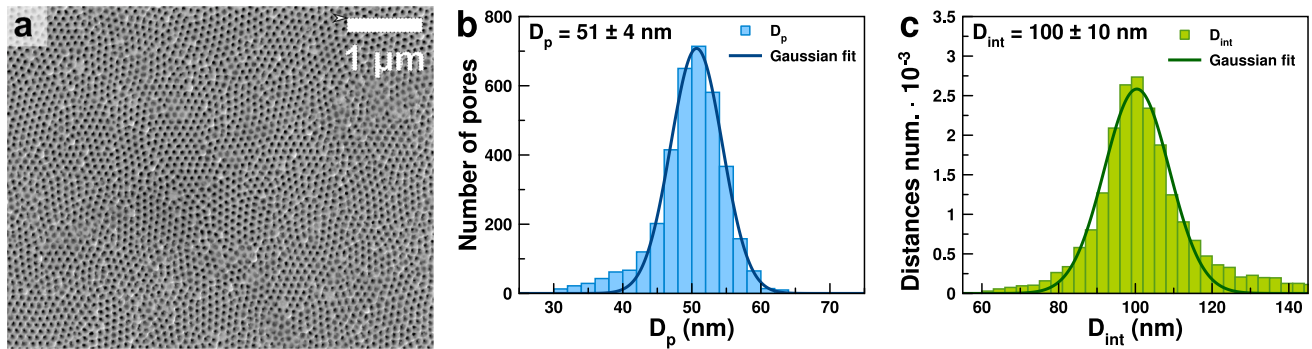


Fig. 2. (a) A top-view SEM image of the AAO template, (b) pore diameter distribution and (c) inter-pore distance distribution.

The coercivity H_c as a function of the nanowire length L for the field applied parallel to the long axis of wires is shown in Fig. 4a. H_c increases non-linearly from 325 to 530 Oe with increasing L . From previous results for MNA, based on Fe [36,37], Ni [38–41], Co [12,42–46], FeNi [47,48], CoFe [49,50,48], NiCoFe [51,52] the observed trend is expected but not predictable, since too many factors play a role in this scenario. For instance, it is clear that the presence of Co with its magnetocrystalline anisotropy can lead to a decrease of the coercivity upon increasing length. However, in CoFe₂ nanowires a rise of H_c was observed [49], whereas in NiFe [47] and some CoFeB [38] nanowires with easy axis parallel to the wire, a decreasing trend was revealed.

In the case of Fe-based MNA, magnetocrystalline and magnetoelastic terms are negligible and, thus, the observed magnetic properties are the result of a competition between shape anisotropy and magnetostatic interactions. In order to describe the behavior of coercivity in a magnetic field parallel to the nanowires, a model of long interacting nanowires was applied [49,53,54]. According to this model, the macroscopic coercivity H_c can be expressed as a function of the length L as follows:

$$H_c = H_0 \left(1 - \sqrt{\frac{\epsilon M_S D_p^2}{4 H_0 D_{int} L} \left(1 - \frac{1}{\sqrt{1 + \frac{L^2}{D_{int}^2}}} \right)} \right), \quad (2)$$

where H_0 is the coercivity of an infinitely long isolated nanowire, $M_S = 21.3$ kOe is the saturation magnetization of bulk Fe, ϵ is a parameter that depends mostly on the arrangement of the magnetic wires and takes account of an energy barrier, which decreases due to magnetization reversal of the wires [49], induced by interactions, $D_p = 52$ nm and $D_{int} = 100$ nm.

The best fit of the experimental data using Eq. (2) (solid line in Fig. 4a) yields the following parameters: $H_0 = 615 \pm 38$ Oe and $\epsilon = 3 \pm 1$. Additionally, the value obtained by Qin et al. [55] for the similar

nanowire array was also plotted in Fig. 4a. Thus, the experimental data are in good agreement with the used model.

Non-monotonic behaviour of coercivity for the short wires is most likely connected with inhomogeneities of the wires like diameter deviation, defects of the structure, and so on, which are more crucial for the smaller length. Besides that, as it was mentioned above, there is significant length deviation for three samples (with the largest errors for the samples with nanowires shorter than 7 μ m), but only one of them strongly deviates from the common trend, supposing weak dependence of coercivity on the small deviation. This finding confirms the results for Ni nanowires, where such deviation does not lead to strong longitudinal coercivity changes for the average sample length of about 7 μ m [56].

The coercivity of an isolated nanowire can be obtained by an analytical model. The nanowire reversal mode is governed by a domain wall, which arises in nanowire during remagnetization. The domain wall type is in turn determined by the exchange length ($l_{exch} = \sqrt{2A/(\mu_0 M_S^2)}$) to nanowire diameter D_p ratio, where A is the exchange stiffness constant and μ_0 is the vacuum permeability. For 50 nm diameter Fe nanowires, $l_{exch}/D_p \approx 15$. In this case, one can apply the model of vortex domain wall (VDW) [57,58]. The Vortex length L_v is given by (we have found that phenomenological factor 1/14 leads to better agreement between experiment and model in Ref. [57] than the original 1/30 one):

$$L_v = \frac{0.18 D_p^2}{\sqrt{10} l_{exch}} \frac{1}{\sqrt{1 - \frac{1}{14} \left(\frac{D_p}{\Delta_z} \right)^2}}, \quad (3)$$

where $\Delta_z = \sqrt{A/(\mu_0 M_S H)}$. The denominator of Eq. (3) is zero for a certain field and hence the vortex length becomes infinite. This field value is defined as nanowire coercivity. The calculated coercivity $H_0 = 630$ Oe is close to the fitted value [29,59]. This confirms that the remagnetization process is governed by the motion of VDW.

The results obtained for the perpendicular field-to-wire orientation

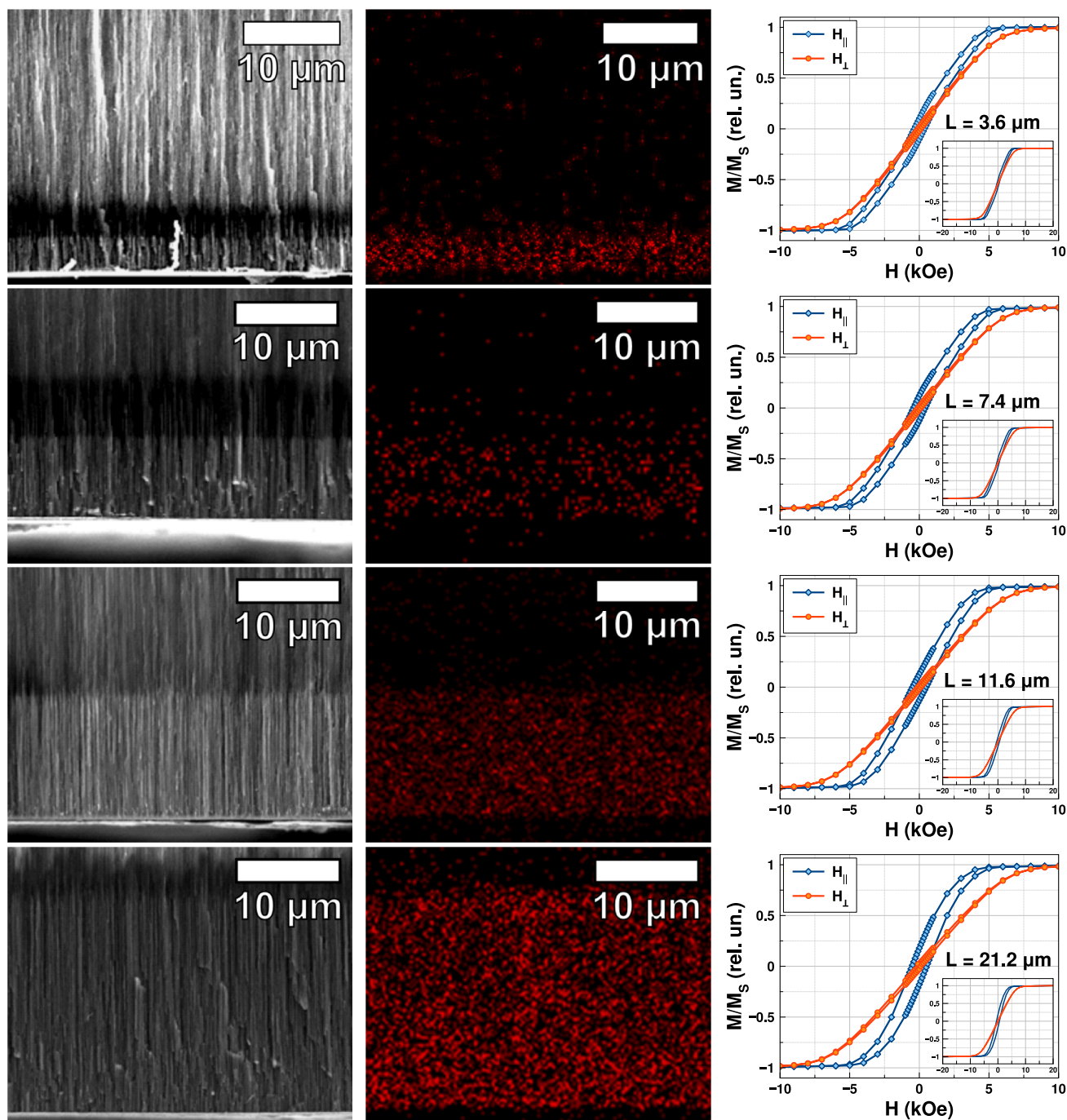


Fig. 3. Cross-sectional SEM images (left column), EDX maps of corresponding cross-sections (central column), and magnetization reversal curves (right column) of the Fe/AAO nanocomposites with various length of nanowires.

also demonstrate the increasing trend (Fig. 4b), although the range is four times smaller than for the parallel case.

Correlated with coercivity, the squareness also increases with the length when the field is applied parallel to the long axis of the nanowires (Fig. 5a). This is in agreement with a decreasing interaction, which is in the base of the used model.

For the perpendicular field direction the squareness changes almost randomly (Fig. 5b), but the absolute values are so small that relative changes can be too high. This deviation can be caused by a small misalignment of the angle between the wires and field leading to a significant parallel projection of the field direction.

The contribution of the shape anisotropy can easily be revealed by integral magnetization measurements, whereas the interactions can not

be probed in the same manner. A widely used approach in order to understand the magnetostatic interactions accurately is to determine the first order reversal curves (FORC). Based on the Moving Preisach Model (MPM) [60], FORC distributions obtained for nanocomposites with nanowires of different lengths were analyzed. It is worth to note that a FORC diagram which is measured experimentally does not unambiguously correspond to the Preisach distributions of switching and interaction fields [61]. Nevertheless, one can use FORC to perform qualitative analysis and analyze its dependence on the system parameters (e.g. with length changing).

FORC results are shown in Fig. 6. All figures demonstrate a narrow distribution along the H_c^F axis and a broad one along the H_u axis. Closed contours are considered as indicators of a single-domain behaviour. This

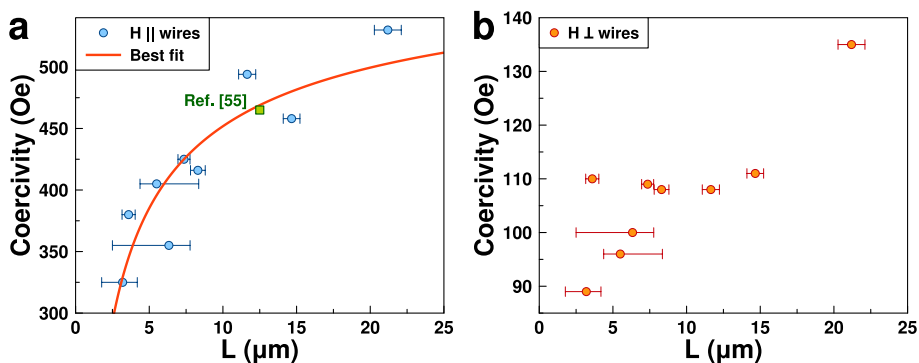


Fig. 4. Length dependence of coercivity H_c for the field applied parallel (a) and perpendicular (b) to the long axis of nanowires.

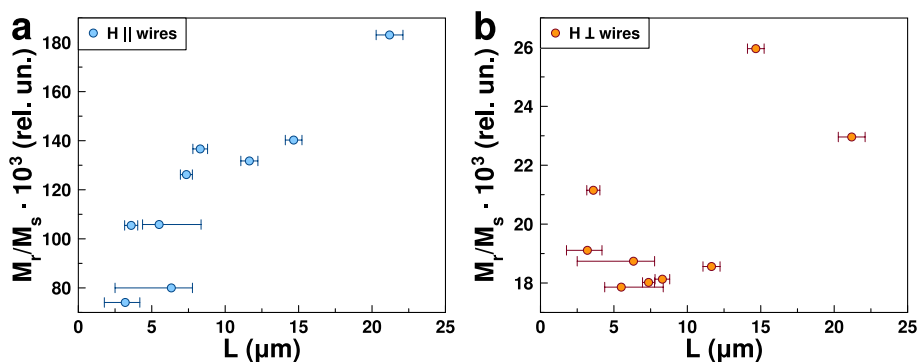


Fig. 5. Squareness of the remagnetization curve of MNA as a function of the nanowire length for the field applied parallel (a) and perpendicular (b) to the long axis of the nanowires.

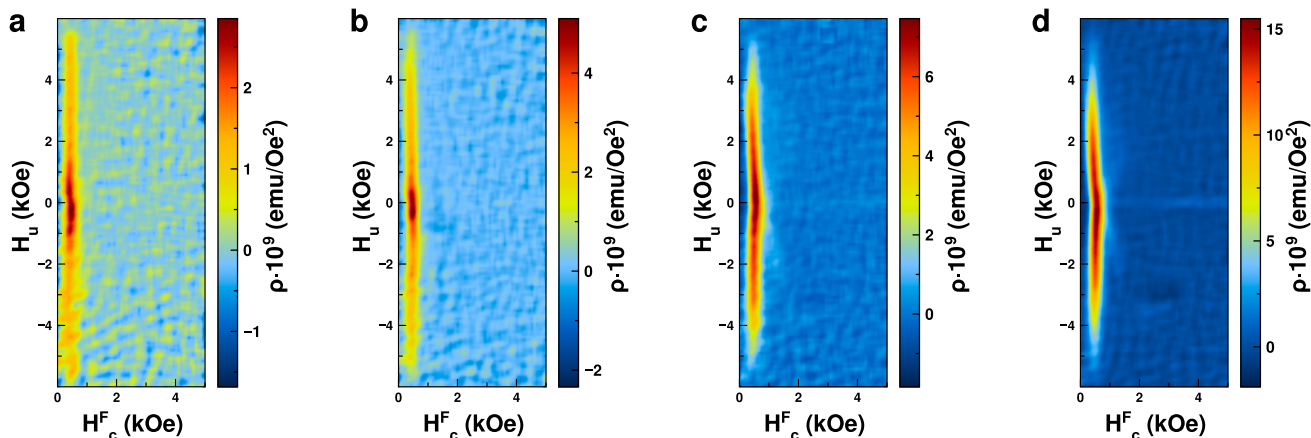


Fig. 6. FORC distribution for the Fe/AAO nanocomposites with the nanowire length of 3.6 μm (a), 7.4 μm (b), 11.6 μm (c), 21.2 μm (d).

conclusion is supported by the fact that single-domain nanowires are magnetized most likely by vortex propagation [62] (in agreement with the results discussed above). Besides that, the critical single-domain radius for Fe wires of considered aspect ratio is much larger than their diameter [9]. However, we have to emphasize that since we did not perform any studies of an individual nanowire, the presented pieces of evidence of single-domain behaviour are rather indirect ones.

Fig. 7a displays the FORC distribution along H_c^F at $H_u = 0$. This dependence is well fitted by a Gaussian function with a HWHM of about 200 Oe. The peak position of the distribution as function of the length is presented in Fig. 7b. It also increases upon the length like the array coercivity H_c , indicating a growth of individual nanowire switching field. This growth occurs abruptly demonstrating some critical length

near 10–11 μm . Generally speaking, the FORC distribution does not coincide with the Moving Preisach Model distribution since interactions can cause changes in switching field values [61]. Probably, the change of the interaction mode leads to a sharp transition with length. Additionally, length deviation affects the interactions and should lead to “ridge”-like features in FORC-diagrams, which we do not observe in Fig. 6, confirming uniform length distribution.

The distribution of H_u taken as a cross-section of FORC diagram at the corresponding peak position is shown in Fig. 7c. Some intensity occurs between -6 and 6 kOe for all measured lengths, indicating mean-field interactions. At the same time, local interactions manifest themselves by additional narrower peak near $H_u = 0$. This peak can arise due to higher relative deviation of the length from the average value, which is more significant for shorter wires [56]. For longer wires, mean field

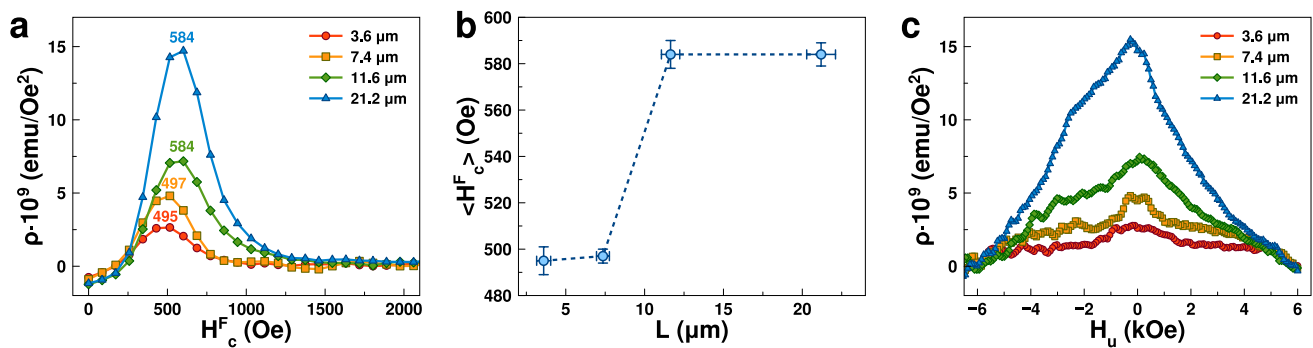


Fig. 7. FORC distribution along H_c^F axis (a), length dependence of H_c^F peak position (b), and FORC distribution along H_u axis.

interactions mostly dominate. The width of the distribution is a measure of interactions in the saturated state [63] and it decreases from about 11 kOe to 5 kOe with length agreeing with integral coercivity behavior. Higher intensity at negative values emphasizes a demagnetizing character of the interactions usual for nanowire arrays.

4. Conclusions

Magnetic nanowire arrays made of Fe nanowires possessing constant diameter and interwire distance, but a length varying from 3.6 to 21.2 μm were synthesized. It has been demonstrated that the length dependence of coercivity is well described by the model of long interacting nanowires, with interactions decreasing with length. An estimation of the coercivity of an isolated wire has shown that the remagnetization process occurs likely via vortex domain wall motion. Analysis of the first order reversal curves has revealed that the wires demonstrate single-domain behavior with narrow switching field distribution. Local interactions presented in short wires concede to mean field interaction with increasing length. A decrease in width of the H_u distribution additionally confirms a reduction of the interactions.

CRedit authorship contribution statement

A.H.A. Elmekawy: Formal analysis, Investigation, Writing - original draft, Visualization. **E. Iashina:** Formal analysis, Writing - original draft. **I. Dubitskiy:** Formal analysis, Writing - review & editing. **S. Sotnichuk:** Resources, Investigation, Writing - review & editing. **I. Bozhev:** Resources. **D. Kozlov:** Resources, Investigation. **K. Napolskii:** Resources, Investigation, Writing - review & editing. **D. Menzel:** Investigation, Resources. **A. Mistonov:** Conceptualization, Writing - review & editing, Supervision.

Declaration of Competing Interest

The authors declare that they have no known competing financial interests or personal relationships that could have appeared to influence the work reported in this paper.

Acknowledgement

The work was supported by Russian Science Foundation (project No. 18-72-00011). The authors are grateful to the Research Park of St. Petersburg State University and the staff of the resource centers “Nanotechnologies” (<http://nano.spbu.ru>), “X-ray diffraction methods of research” (<http://xrd.spbu.ru>), and “Innovative technologies of composite nanomaterials” (<https://nanocomposites.spbu.ru/>) V. Kalganov, I. Kasatkin and D. Nazarov, respectively, for their invaluable contribution in obtaining experimental data. “Educational and Methodical Center of Lithography and Microscopy” (Lomonosov Moscow State University Research Facilities Sharing Centre) was used for

the preparation of current collectors. SS and KN are grateful for the support of the Interdisciplinary Scientific and Educational School of Moscow University “Future Planet: Global Environmental Change”.

References

- [1] J. Um, M.R. Zamani Kouhpanji, S. Liu, Z. Nematı Porshokouh, S. Sung, J. Kosel, B. Stadler, Fabrication of long-range ordered aluminum oxide and Fe/Au multilayered nanowires for 3-d magnetic memory, *IEEE Trans. Magn.* 56 (2) (2020) 1–6, <https://doi.org/10.1109/TMAG.2019.2942946>.
- [2] S. Parkin, S.-H. Yang, Memory on the racetrack, *Nat. Nanotechnol.* 10 (3) (2015) 195–198, <https://doi.org/10.1038/nnano.2015.41>.
- [3] M.R. Zamani Kouhpanji, B.J.H. Stadler, A guideline for effectively synthesizing and characterizing magnetic nanoparticles for advancing nanobiotechnology: A review, *Sens.* 20 (9), <https://doi.org/10.3390/s20092554>. URL: <https://www.mdpi.com/1424-8220/20/9/2554>.
- [4] K.S. Napolskii, I.V. Roslyakov, A.A. Eliseev, D.I. Petukhov, A.V. Lukashin, S.-F. Chen, C.-P. Liu, G.A. Tsirlina, Tuning the microstructure and functional properties of metal nanowire arrays via deposition potential, *Electrochim. Acta* 56 (5) (2011) 2378–2384.
- [5] I. Cabria, V. Prida, Magnetostatic dipolar anisotropy energy and anisotropy constants in arrays of ferromagnetic nanowires as a function of their radius and interwall distance, *J. Phys. Commun.* 4 (3) (2020), 035015.
- [6] Y. Guerra, R. Peña-García, A. do Nascimento-Junior, B.C. Viana, E. Padrón-Hernández, Length distribution effects on the dipolar interactions for hexagonal arrays of nine nanowires, *J. Magn. Magn. Mater.* 506 (2020) 166797. <https://doi.org/10.1016/j.jmmm.2020.166797>. URL: <http://www.sciencedirect.com/science/article/pii/S0304885319339393>.
- [7] L. Hong-Jian, Y. Ming, W. Qiong, P. Yi, L. Yu-Qing, L. Wei-Qiang, Z. Dong-Tao, Z. Jiu-Xing, Effects of dipolar interactions on magnetic properties of Co nanowire arrays, *Chin. Phys. B* 26 (11) (2017), 117503, <https://doi.org/10.1088/1674-1056/26/11/117503>.
- [8] E. Kantar, Geometry-dependent magnetic properties of Ising-type multisegment nanowires, *J. Supercond. Novel Magn.* 29 (10) (2016) 2699–2704, cited by 1. <https://doi.org/10.1007/s10948-016-3603-2>. URL: <https://www.scopus.com/inward/record.uri?eid=2-s2.0-84976354850&doi=10.1007%2fs10948-016-3603-2&partnerID=40&md5=5ea7192eeec7e10a792d08942f78e9b>.
- [9] L. Sun, Y. Hao, C.-L. Chien, P.C. Searson, Tuning the properties of magnetic nanowires, *IBM J. Res. Dev.* 49 (1) (2005) 79–102.
- [10] L. Qin, J. Zhao, Q. Guo, Z. Yan, F. Mu, P. Chen, G. Li, Effect of length on the magnetic properties of ni 300 nm wide nanowires, *Phys. E* 50 (2013) 17–21.
- [11] X. Xu, G. Zangari, Microscopic structure and magnetic behavior of arrays of electrodeposited ni and fe nanowires, *J. Appl. Phys.* 97 (10) (2005) 10A306.
- [12] M. Vázquez, L.G. Vivas, Magnetization reversal in Co-base nanowire arrays, *Physica Status Solidi (b)* 248 (10) (2011) 2368–2381. <https://doi.org/10.1002/pssb.201147092>. URL: <https://onlinelibrary.wiley.com/doi/abs/10.1002/pssb.201147092>.
- [13] A. Ochoa, J. Mejía-López, E. Velásquez, J. Mazo-Zuluaga, Finite-length fe nanowire arrays: the effects of magnetic anisotropy energy, dipolar interaction and system size on their magnetic properties, *J. Phys. D: Appl. Phys.* 50 (9) (2017), 095003.
- [14] E. Yoo, A.Y. Samardak, Y.S. Jeon, A.S. Samardak, A.V. Ognev, S.V. Komogortsev, Y. K. Kim, Composition-driven crystal structure transformation and magnetic properties of electrodeposited Co–W alloy nanowires, *J. Alloy. Compd.* 843 (2020), 155902, <https://doi.org/10.1016/j.jallcom.2020.155902>. URL: <http://www.sciencedirect.com/science/article/pii/S0925838820322660>.
- [15] S. Khan, N. Ahmad, A. Safeer, A. Hassan, S. Zareen, J. Iqbal, Structural, magnetic and electrical investigations of $\text{Fe}_{1-x}\text{Mn}_x$ ($0 \leq x \leq 0.39$) alloy nanowires via electrodeposition in AAO templates, *Solid State Sci.* 107 (2020), 106351, <https://doi.org/10.1016/j.solidstatesciences.2020.106351>. URL: <http://www.sciencedirect.com/science/article/pii/S1293255819314499>.
- [16] N. Ahmad, M.Z. Shafiq, S. Khan, W.H. Shah, I. Murtaza, A. Majid, K. Javed, Dominance of shape anisotropy among magnetostatic interaction and magnetocrystalline anisotropy in electrodeposited $(\text{FeCo})_{1-x}\text{Cu}_x$ ($x = 0.1 - 0.5$)

- ternary alloy nanowires, *J. Supercond. Novel Magn.* 33 (5) (2020) 1495–1505, <https://doi.org/10.1007/s10948-019-05394-0>.
- [17] R. Dost, Y. Zhou, H. Zhang, D. Allwood, B. Inkson, Effect of annealing on the electrical and magnetic properties of electrodeposited Ni and permalloy nanowires, *J. Magn. nd Magn. Mater.* 499. <https://doi.org/10.1016/j.jmmm.2019.166276>. URL: <https://www.scopus.com/inward/record.uri?eid=2-s2.0-85076355765&doi=10.1016%2Fj.jmmm.2019.166276&partnerID=40&md5=6aa8370cdbc558d080ef0c345d2f5b2>.
- [18] J. Xu, J. Wang, B. Hong, X. Peng, X. Wang, H. Ge, J. Hu, Growth and magnetic interaction of single crystalline Ni gradient-diameter magnetic nanowire arrays, *J. Mater. Sci.* 54 (17) (2019) 11538–11545, <https://doi.org/10.1007/s10853-019-03694-3>. URL: <https://www.scopus.com/inward/record.uri?eid=2-s2.0-85066492844&doi=10.1007%2Fs10853-019-03694-3&partnerID=40&md5=097939c01eb713f482473531eca44620>.
- [19] J. Kan, M. Lubarda, K. Chan, V. Uhlir, A. Scholl, V. Lomakin, E. Fullerton, Periodic chiral magnetic domains in single-crystal nickel nanowires, *Phys. Rev. Mater.* 2 (6). <https://doi.org/10.1103/PhysRevMaterials.2.064406>. URL: <https://www.scopus.com/inward/record.uri?eid=2-s2.0-85055874893&doi=10.1103%2FPhysRevMaterials.2.064406&partnerID=40&md5=dfd8fe7481d6de87a681c037c26228fb>.
- [20] S.N. Kozlov, O.V. Skryabina, S.V. Egorov, I.A. Golovchanskiy, A.A. Klimenko, K.S. Napolskii, V.S. Stolyarov, Magneto-resistance of a single polycrystalline nickel nanowire, *J. Appl. Phys.* 125 (6) (2019) 063902. <https://doi.org/10.1063/1.5064680>.
- [21] O.V. Skryabina, S.N. Kozlov, S.V. Egorov, A.A. Klimenko, V.V. Ryazanov, S. V. Bakurskiy, M.Y. Kupriyanov, N.V. Klenov, I.I. Soloviev, A.A. Golubov, K. S. Napolskii, I.A. Golovchanskiy, D. Roditchev, V.S. Stolyarov, Anomalous magneto-resistance of Ni-nanowire/Nb hybrid system, *Sci. Rep.* 9 (1) (2019) 14470, <https://doi.org/10.1038/s41598-019-50966-8>.
- [22] S. Agarwal, M. Khatri, Effect of pH and boric acid on magnetic properties of electrodeposited Co nanowires, *Proc. Natl. Acad. Sci. India A* <https://doi.org/10.1007/s40010-020-00708-7>. URL: <https://www.scopus.com/inward/record.uri?eid=2-s2.0-85089382262&doi=10.1007%2Fs40010-020-00708-7&partnerID=40&md5=ad43cbf84d4848e26a6e15f4438d6f0f3>.
- [23] K. Nath, J. Sinha, S. Banerjee, Flipping anisotropy and changing magnetization reversal modes in nano-confined cobalt structures, *J. Magn. Magn. Mater.* 476 (2019) 412–416, <https://doi.org/10.1016/j.jmmm.2018.12.093>. URL: <https://www.scopus.com/inward/record.uri?eid=2-s2.0-85059568069&doi=10.1016/j.jmmm.2018.12.093&partnerID=40&md5=8e825069f7de211994b0ed842b9fb46a1>.
- [24] H. Zhang, W. Jia, H. Sun, L. Guo, J. Sun, Growth mechanism and magnetic properties of Co nanowire arrays by ac electrodeposition, *J. Magn. Magn. Mater.* 468 (2018) 188–192, <https://doi.org/10.1016/j.jmmm.2018.08.013>. URL: <https://www.scopus.com/inward/record.uri?eid=2-s2.0-85051259484&doi=10.1016/j.jmmm.2018.08.013&partnerID=40&md5=ed91e9fa44380d38748b233f0fe3009>.
- [25] I. Doludenko, D. Zagorskii, K. Frolov, I. Perunov, M. Chuev, V. Kanevskii, N. Erokhina, S. Bedin, Nanowires made of FeNi and FeCo alloys: Synthesis, structure, and Mössbauer measurements, *Phys. Solid State* 62 (9) (2020) 1639–1646, <https://doi.org/10.1134/S1063783420090061>. URL: <https://www.scopus.com/inward/record.uri?eid=2-s2.0-85090899495&doi=10.1134/S1063783420090061&partnerID=40&md5=3b62ac042feba559c3d36fe03ed70a33>.
- [26] H. Cesiulis, N. Tsytaru, E. Podlaha, D. Li, J. Sort, Electrodeposition of iron-group alloys into nanostructured oxide membranes: Synthetic challenges and properties, *Curr. Nanosci.* 15 (1) (2019) 84–99, <https://doi.org/10.2174/1573413714666180410154104>. URL: <https://www.scopus.com/inward/record.uri?eid=2-s2.0-85062818018&doi=10.2174/1573413714666180410154104&partnerID=40&md5=02c0174a5499d05187bdde87a648ac92>.
- [27] F. Noori, A. Ramazani, M. Almasi Kashi, Controlling structural and magnetic properties in CoNi and CoNiFe nanowire arrays by fine-tuning of Fe content, *J. Alloys Compd.* 756 (2018) 193–201, <https://doi.org/10.1016/j.jallcom.2018.04.261>. URL: <https://www.scopus.com/inward/record.uri?eid=2-s2.0-85046832519&doi=10.1016/j.jallcom.2018.04.261&partnerID=40&md5=3142bd81fe8286e2fc551359255a5722>.
- [28] A.S. Goncharova, S.V. Sotnichuk, A.S. Semisalova, T.Y. Kiseleva, I. Sergueev, M. Herlitschke, K.S. Napolskii, A.A. Eliseev, Oriented arrays of iron nanowires: synthesis, structural and magnetic aspects, *J. Sol-Gel. Sci. Technol.* 81 (2) (2017) 327–332.
- [29] A. Elmekawy, E. Iashina, I. Dubitskiy, S. Sotnichuk, I. Bozhev, K.S. Napolskii, D. Menzel, A. Mistonov, Magnetic properties and force analysis of iron nanowire arrays, *Mater. Today Commun.* 25 (2020), 101609.
- [30] M. Lillo, D. Losic, Pore opening detection for controlled dissolution of barrier oxide layer and fabrication of nanoporous alumina with through-hole morphology, *J. Membr. Sci.* 327 (1) (2009) 11–17, <https://doi.org/10.1016/j.memsci.2008.11.033>. URL: <http://www.sciencedirect.com/science/article/pii/S0376738808010089>.
- [31] I.V. Roslyakov, D.S. Koshkodaev, A.A. Eliseev, D. Hermida-Merino, V.K. Ivanov, A. V. Petukhov, K.S. Napolskii, Growth of porous anodic alumina on low-index surfaces of Al single crystals, *J. Phys. Chem. C* 121 (49) (2017) 27511–27520.
- [32] I. Mayergoyz, Hysteresis models from the mathematical and control theory points of view, *J. Appl. Phys.* 57 (8) (1985) 3803–3805.
- [33] N. Lupu, Electrodeposited nanowires and their applications, *BoD–Books on Demand* (2010).
- [34] R.J. Harrison, J.M. Feinberg, Forcinel: An improved algorithm for calculating first-order reversal curve distributions using locally weighted regression smoothing, *Geochem. Geophys. Geosyst.* 9 (5).
- [35] Y.P. Ivanov, M. Vázquez, O. Chubykalo-Fesenko, Magnetic reversal modes in cylindrical nanowires, *J. Phys. D: Appl. Phys.* 46 (48) (2013), 485001.
- [36] V. Haehnel, S. Fähler, P. Schaaf, M. Miglierini, C. Mickel, L. Schlörb, Towards smooth and pure iron nanowires grown by electrodeposition in self-organized alumina membranes, *Acta Mater.* 58 (7) (2010) 2330–2337, <https://doi.org/10.1016/j.actamat.2009.12.019>. URL: <http://www.sciencedirect.com/science/article/pii/S1359645409008611>.
- [37] A. Ochoa, J. Mejía-López, E.A. Velásquez, J. Mazo-Zuluaga, Finite-length Fe nanowire arrays: the effects of magnetic anisotropy energy, dipolar interaction and system size on their magnetic properties, *J. Phys. D: Appl. Phys.* 50 (9) (2017), 095003, <https://doi.org/10.1088/1361-6463/aa5763>.
- [38] F. Béron, L. Clime, M. Ciureanu, D. Ménard, R. Cochrane, A. Yelon, Magnetostatic interactions and coercivities of ferromagnetic soft nanowires in uniform length arrays, *J. Nanosci. Nanotechnol.* 8 (6) (2008) 2944–2954.
- [39] M. Vázquez, K. Pirota, J. Torrejón, D. Navas, M. Hernández-Vélez, Magnetic behaviour of densely packed hexagonal arrays of Ni nanowires: Influence of geometric characteristics, *J. Magn. Magn. Mater.* 294 (2) (2005) 174–181, <https://doi.org/10.1016/j.jmmm.2005.03.032>. URL: <http://www.sciencedirect.com/science/article/pii/S030488530500363X>.
- [40] G. Kartopu, O. Yalçın, K.-L. Choy, R. Topkaya, S. Kazan, B. Aktas, Size effects and origin of easy-axis in nickel nanowire arrays, *J. Appl. Phys.* 109 (3) (2011) 033909. <https://doi.org/10.1063/1.3531565>.
- [41] L. Qin, J. Zhao, Q. Guo, Z. Yan, F. Mu, P. Chen, G. Li, Effect of length on the magnetic properties of Ni 300 nm wide nanowires, *Phys. E* 50 (2013) 17–21, <https://doi.org/10.1016/j.physe.2013.02.016>. URL: <http://www.sciencedirect.com/science/article/pii/S1386947713000507>.
- [42] H. Zeng, M. Zheng, R. Skomski, D.J. Sellmyer, Y. Liu, L. Menon, S. Bandyopadhyay, Magnetic properties of self-assembled Co nanowires of varying length and diameter, *J. Appl. Phys.* 87 (9) (2000) 4718–4720, <https://doi.org/10.1063/1.373137>.
- [43] L.G. Vivas, R. Yanes, O. Chubykalo-Fesenko, M. Vazquez, Coercivity of ordered arrays of magnetic Co nanowires with controlled variable lengths, *Appl. Phys. Lett.* 98 (23) (2011) 232507. <https://doi.org/10.1063/1.3597227>.
- [44] A.H. Montazer, A. Ramazani, M. Almasi Kashi, Magnetically extracted microstructural development along the length of Co nanowire arrays: The interplay between deposition frequency and magnetic coercivity, *J. Appl. Phys.* 120 (11) (2016), 113902, <https://doi.org/10.1063/1.4962372>.
- [45] M. Ciureanu, F. Béron, P. Ciureanu, R. Cochrane, D. Ménard, A. Sklyuyev, A. Yelon, First order reversal curves (forc) diagrams of Co nanowire arrays, *J. Nanosci. Nanotechnol.* 8 (11) (2008) 5725–5732.
- [46] G. Kartopu, O. Yalçın, M. Es-Souni, A.C. Başaran, Magnetization behavior of ordered and high density Co nanowire arrays with varying aspect ratio, *J. Appl. Phys.* 103 (9) (2008), 093915, <https://doi.org/10.1063/1.2917191>.
- [47] A. Ramazani, V. Asgari, A. Montazer, M.A. Kashi, Tuning magnetic fingerprints of FeNi nanowire arrays by varying length and diameter, *Curr. Appl. Phys.* 15 (7) (2015) 819–828.
- [48] N. Mansouri, N. Benbrahim-Cherief, E. Chainet, F. Charlot, T. Encinas, S. Boudinar, B. Benfedda, L. Hamadou, A. Kadri, Electrodeposition of equiaxial FeNi and FeCo nanowires: Structural and magnetic properties, *J. Magn. Magn. Mater.* 493 (2020), 165746, <https://doi.org/10.1016/j.jmmm.2019.165746>. URL: <http://www.sciencedirect.com/science/article/pii/S0304885319312259>.
- [49] S. Lim, F. Xu, N. Phuoc, C. Ong, Length dependence of coercivity in CoFe₂ nanowire arrays with high aspect ratios, *J. Alloy. Compd.* 505 (2) (2010) 609–612.
- [50] M. Almasi Kashi, A. Ramazani, A.S. Esmaili, Magnetostatic interaction investigation of CoFe alloy nanowires by first-order reversal-curve diagrams, *IEEE Trans. Magn.* 49 (3) (2013) 1167–1171, <https://doi.org/10.1109/TMAG.2012.2230335>.
- [51] G.C. Han, B.Y. Zong, Y.H. Wu, Magnetic properties of magnetic nanowire arrays, *IEEE Trans. Magn.* 38 (5) (2002) 2562–2564, <https://doi.org/10.1109/TMAG.2002.801952>.
- [52] S. Samanifar, M. Almasi Kashi, A. Ramazani, M. Alikhani, Reversal modes in FeCoNi nanowire arrays: Correlation between magnetostatic interactions and nanowires length, *J. Magn. Magn. Mater.* 378 (2015) 73–83, <https://doi.org/10.1016/j.jmmm.2014.10.155>. URL: <http://www.sciencedirect.com/science/article/pii/S0304885314010786>.
- [53] D. Laroze, J. Escrig, P. Landeros, D. Altir, M. Vázquez, P. Vargas, A detailed analysis of dipolar interactions in arrays of bi-stable magnetic nanowires, *Nanotechnology* 18 (41) (2007), 415708.
- [54] J. Escrig, R. Lavin, J. Palma, J. Denardin, D. Altir, A. Cortes, H. Gomez, Geometry dependence of coercivity in Ni nanowire arrays, *Nanotechnology* 19 (7) (2008), 075713.
- [55] X.F. Qin, C.H. Deng, Y. Liu, X.J. Meng, J.Q. Zhang, F. Wang, X.H. Xu, Magnetization reversal of high aspect ratio iron nanowires grown by electrodeposition, *IEEE Trans. Magn.* 48 (11) (2012) 3136–3139, <https://doi.org/10.1109/TMAG.2012.2205561>.
- [56] M.P. Proenca, C.T. Sousa, J. Ventura, J. Garcia, M. Vazquez, J.P. Araujo, Identifying weakly-interacting single domain states in Ni nanowire arrays by FORC, *J. Alloy. Compd.* 699 (2017) 421–429, <https://doi.org/10.1016/j.jallcom.2016.12.340>. URL: <http://www.sciencedirect.com/science/article/pii/S0925838816342694>.
- [57] S. Bochmann, D. Döhler, B. Trapp, M. Staño, O. Fruchart, J. Bachmann, Preparation and physical properties of soft magnetic nickel-cobalt three-segmented nanowires, *J. Appl. Phys.* 124 (16) (2018), 163907.
- [58] S. Jamet, N. Rougemaille, J.-C. Toussaint, O. Fruchart, Head-to-head domain walls in one-dimensional nanostructures: an extended phase diagram ranging from strips to cylindrical wires, *Magn. Nano Microwires* (2015) 783–811.

- [59] I. Dubitskiy, A. Elmekawy, E. Iashina, S. Sotnichuk, K. Napolskii, D. Menzel, A. Mistonov, Effect of interactions and non-uniform magnetic states on the magnetization reversal of iron nanowire arrays, *J. Supercond. Novel Magn.* <https://doi.org/10.1007/s10948-020-05711-y>.
- [60] E.D. Torre, Measurements of interaction in an assembly of γ -iron oxide particles, *J. Appl. Phys.* 36 (2) (1965) 518–522, <https://doi.org/10.1063/1.1714022>.
- [61] C.-I. Dobrotă, A. Stancu, What does a first-order reversal curve diagram really mean? A study case: Array of ferromagnetic nanowires, *J. Appl. Phys.* 113 (4) (2013), 043928.
- [62] R. Hertel, Computational micromagnetism of magnetization processes in nickel nanowires, *J. Magn. Magn. Mater.* 249 (1) (2002) 251–256, [https://doi.org/10.1016/S0304-8853\(02\)00539-5](https://doi.org/10.1016/S0304-8853(02)00539-5). URL: <http://www.sciencedirect.com/science/article/pii/S0304885302005395>.
- [63] C. Carvallo, Özdemir, D.J. Dunlop, First-order reversal curve FORC diagrams of elongated single-domain grains at high and low temperatures, *J. Geophys. Res.* 109 (B4). <https://doi.org/10.1029/2003JB002539>.